Journal of Materials Chemistry

Dynamic Article Links

Cite this: *J. Mater. Chem.*, 2011, **21**, 17104

www.rsc.org/materials

PAPER

Synthesis of hydrophobic layered luminescent films: Organic–inorganic hybrid mono-n-dodecyloxy-phosphinyl-cerium (terbium)

Qiuling Luo,[a] Guanzhong Lu,*[ab] Shaodian Shen,[b] Xiuzhen Xiao,[b] Dongsen Mao[b] and Yanqin Wan[a]

Received 8th June 2011, Accepted 27th July 2011
DOI: 10.1039/c1jm12601f

With hydrophobic properties and ordered layered structures, mono-n-dodecyloxy-phosphinyl-cerium (terbium) (MDPCT) organic–inorganic hybrid materials were synthesized using cerium nitrate, terbium nitrate and mono-n-dodecyl phosphate (MDP) surfactant with three functions, hydrophobic group and phosphorus precursor, and characterized by XRD, SEM, TEM, FTIR and PLS. The results show that the solvent affects the interlayer spacing, crystallization and luminescent intensity of the prepared MDPCT materials. MDPCT prepared in water exhibits a more ordered layered structure and a higher degree of crystallinity, as well as stronger luminescent intensity than that prepared in ethanol. Based on the excellent solubility in organic solvents, this MDPCT hybrid luminescent material will be a promising candidate for potential biomedical applications in fluorescent imaging and analysis.

Introduction

Inorganic–organic hybrid materials with "organically-templated inorganic solids" structure have great potential for a variety of applications, including in catalysis, materials science and photo- and electrochemical devices.[1–4] The inorganic and organic species on the nanometre scale can create a homogenous composite, possessing advantageous physicochemical properties.[5,6] Thus, the development of novel materials with functionalities such as catalytic, optical, electronic, magnetic, and dielectric properties has been focused on the design and fabrication of the inorganic species, including metal, oxide, and oxyanion-based inorganic components.[3,7–10]

Lanthanide-doped organic–inorganic hybrid materials have gained much attention as optical materials. In the early days, interest relied on the possibility of combining the properties of sol–gel host materials with the well-known luminescence of lanthanide ions (Ln).[11–20] More recently, with the rapid development of photonic hybrid materials, multifunctional Ln-hybrid nanocomposites have been championed and play an important role in bio-sensors, bio-analytics and even clinical imaging diagnostics.[21–24] Lanthanide luminescent hybrids are promising candidates for time-resolved fluoroimmunoassays, DNA hybridisation assays, fluorescence imaging microscopy, or *in vivo* imaging.[25–27] Therefore, the design and synthesis of novel optically active Ln-hybrid nanocomposites are of considerable interest based on these promising applications.

Among many rare earth ions, as the main components of blue and green phosphors, Ce^{3+} and Tb^{3+} ions are remarkable. For instance, as efficient green phosphors, the Ce^{3+} and Tb^{3+} ion-doped $LnPO_4$ (Ln = Y, La) bulk powders have been extensively applied in fluorescent lamps, cathode ray tubes (CRTs), and plasma display panels (PDPs).[28–30] Hence, the energy transfer (ET) processes between Ce^{3+} and Tb^{3+} in these micrometre-sized hosts (bulk powders) have been intensively investigated.[31–34] Surprisingly, there are comparatively few investigations into synthesizing cerium (terbium) phosphate organic–inorganic hybrid materials *via* phosphate-based surfactants.

Mono-n-dodecyl phosphate, $(C_{12}H_{25}O)P(O)(OH)_2$(MDP), as a structure-directing template, has been used to successfully prepare aluminophosphate, calcium phosphate and phosphotungstate organic–inorganic hybrid materials.[5,35–37] In this paper, we have prepared the first mono-n-dodecyloxy-phosphinyl-cerium (terbium) (MDPCT) hybrid luminescent materials, in which MDP was used as both phosphorus source and structural template. Due to the layered lipid structure like that of a cell membrane phospholipid, low toxicity compared with organic dyes, and convenient preparation method at room temperature, the MDPCT hybrid luminescent materials will have potential application as a new generation of imaging agents and fluorescent indicators in biomedicine.

Experimental

Preparation of materials

Deionized water or ethanol was used as the solvent. 1 g mono-n-dodecyl phosphate ($(C_{12}H_{25}O)P(O)$-$(OH)_2$, MDP, Lancaster, UK) was dissolved in 20 ml solvent, followed by stirring for 1 h. Then 1.55 g $Ce(NO_3)_3 \cdot 6H_2O$ and 0.085 g $Tb(NO_3)_3 \cdot 6H_2O$

[a]*Key Laboratory for Advanced Materials and Research Institute of Industrial Catalysis, East China University of Science and Technology, Shanghai, 200237, P. R. China. E-mail: gzhlu@ecust.edu.cn; Fax: +86-21-64253703; Tel: +86-21-64252923*
[b]*Research Institute of Applied Catalysis, Shanghai Institute of Technology, Shanghai, 200235, P. R. China*

(Ce : Tb = 95 : 5, mol) was dissolved in 5 ml of the same solvent, and this solution was added dropwise to the MDP solution above. After stirring for 10 min, the mixed solution separated into two layers. The superstratum was the white powder (MDPCT), and the underlayer was a clear solution. After filtration, the obtained white powder was dried at 60 °C, and was already insoluble in polar solvents (such as water and ethanol). The sample was named according to the solvent: MDPCT(W) obtained in water, and MDPCT(E) in ethanol. The synthesis reaction formulae are shown in Fig. 1, and chemical combination of Tb^{3+} with $C_{12}H_{25}OP(O)O_2^{2-}$ is the same as that of Ce^{3+}. Bulk $CePO_4$: Tb was prepared using $Ce(NO_3)_3 \cdot 6H_2O$,Tb-$(NO_3)_3 \cdot 6H_2O$ and H_3PO_4 (H_3PO_4 : (95%Ce + 5%Tb) = 1 : 1, mol) as the raw materials under identical conditions in water.

Characterization of samples

Powder X-ray diffraction (XRD) patterns were recorded on a PANalytical X'Pert Pro Diffractometer with Cu-Kα radiation (λ = 0.15346 nm). Transmission electron microscopy (TEM) images were obtained on a JEOL JEM-2100 microscope operated at 200 kV, and the sample to be measured was first dispersed in ethanol and then collected using copper grids covered with carbon film. Scanning electron microscopy (SEM) images were obtained on a HITACHI S-3400 microscope operated at 20 kV. FT-IR spectra were obtained on a Nicolet 6700 FT-IR spectrometer. The sample to be measured was ground with KBr and pressed into a thin wafer. Photoluminescence spectra were recorded on a Varian Cary Eclipse Fluorescence Spectrophotometer at room temperature equipped with a 150 W Xe lamp in the range of 200–800 nm with a resolution of 1 nm.

Results and discussion

The small-angle XRD patterns of MDP, MDPCT(W) and MDPCT(E) are shown in Fig. 2. The results show that the ordered lamellar structure of the MDP template is evident based on the sharp reflections at 3.4°, 6.8° and 10.1° corresponding to the (100), (200) and (300) reflections; the diffraction peaks of MDPCT(W) are located at 2.5°, 5.0° and 7.5° and the peaks of MDPCT(E) are at 2.95°, 5.86° and 8.75°, which means that the secondary and tertiary structures in the samples are unchanged, and the prepared organic–inorganic hybrid MDPCT materials are of the highly ordered layered structure.[8]

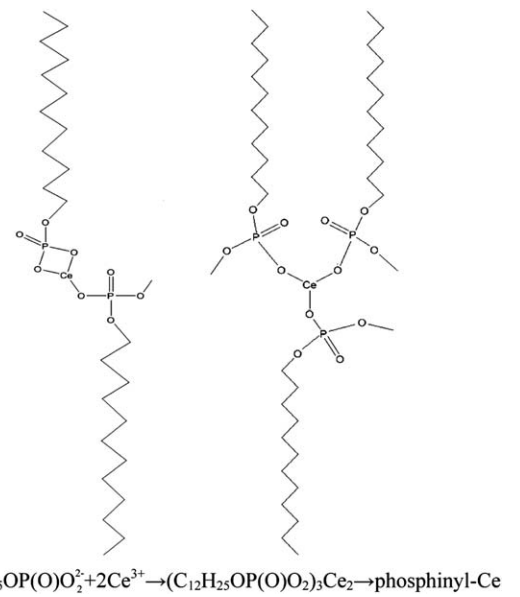

Fig. 1 Two reaction formulae for central Ce^{3+} bonding to $C_{12}H_{25}OP(O)O_2^{2-}$.

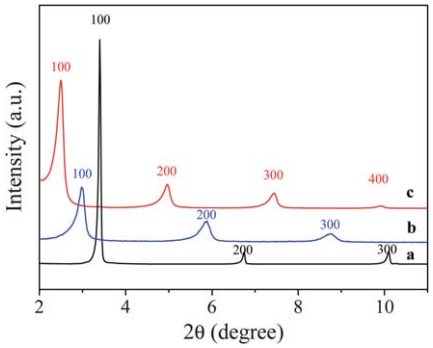

Fig. 2 Small-angle XRD patterns of (a) MDP, (b) MDPCT(E), and (c) MDPCT(W).

The small-angle XRD results show that, with different solvents, the prepared MDPCT samples exhibit different reflections of (100), (200) and (300), including different intensities and positions, which results in the different *d*-spacings. The d_{100}-spacings of three samples are presented in Table 1, and d_{100}-spacing of MDP is 2.5 nm, MDPCT(W) is 3.4 nm and MDPCT (E) is 2.9 nm. Using the same surfactant, MDP, the MDPCT samples with different inter-lamellar spacing can be prepared, which is attributed to a change in the conformation or degree of overlap in the hydrophobic regions, due to different solvents.

From Fig. 3, we can see a change in the hydrophobic regions in different solvents. Based on the similarity theory and intermiscibility, a more polar solvent gives rise to a larger *d*-spacing, due to a stronger interaction between the polar solvent and the polar groups of the MDP surfactant. Therefore, the inter-lamellar spacing of MDPCT(W) (Fig. 3a) is larger than that of MDPCT (E) (Fig. 3b). The small-angle X-ray diffraction peaks of MDPCT(W) are stronger than those of MDPCT(E), which shows MDPCT(W) displays a more highly ordered lamella structure than MDPCT(E). These results are similar to that reported by Fröba for lamella aluminophosphates prepared with a dodecylphosphate template.[29]

Fig. 4 shows the wide-angle XRD pattern of MDP, MDPCT and bulk $CePO_4$. The organic MDP surfactant has the main diffraction peaks at 2θ = 15–35°. The XRD pattern of bulk $CePO_4$ exhibits the diffraction peaks of the hexagonal phase (JCPDS 04-0632).[38] Compared with MDPCT(E), which is almost amorphous, the diffraction peaks of MDPCT(W) have higher intensities.

MDPCT(W) displays the same diffraction peaks (100, 101, 110, 200, 102 *etc.*) as that of hexagonal phase bulk $CePO_4$. Although the positions of the diffraction peaks of MDPCT(E) are the same as that of MDPCT(W), the diffraction peaks of MDPCT(E) are very weak, which reveals that crystallization of phosphinyl-ceriumc(terbium) in water is better than in ethanol. Thus, a highly polar solvent is beneficial for the interaction of

Table 1 The d_{100} spacings of samples

Sample	Peak (100) 2θ (degree)	d_{100} spacing (nm, XRD)	Inter-lamellar spacing (nm, TEM)
MDP	3.40	2.5	
MDPCT(E)	2.99	2.9	3.4
MDPCT(W)	2.51	3.4	3.8

Ln^{3+} and the hydrophilic group of MDP. Two wide peaks at 17.9° and 23.7° in Fig. 4b might be ascribed to a change of hydrophobic regions. For MDPCT(E), the wide peak at 17.9° shifts to 18.5° compared with MDPCT(W), and the peak at 23.7° is not obvious. The results above suggest that different solvents can cause hydrophobic regions to vary, and the ordered layered structure of MDPCT(E) is weaker than that of MDPCT(W).

Fig. 5 shows the TEM images of the MDPCT hybrid materials, and the regularly spaced parallel layers of MDPCT can be clearly observed. The inter-lamellar spacing of MDPCT(W) is 3.8 nm (Fig. 5b), that of MDPCT(E) is 3.4 nm (Fig. 5d), which is in good agreement with the results calculated from the XRD testing (Table 1). The wall of phosphinyl-cerium (terbium) in MDPCT(W) is a little clearer and of a deeper shade than that of MDPCT(E), which coincides with better crystallization in the wide angle XRD pattern of MDPCT(W).

The SEM image (Fig. 6a) of the MDP template shows a smooth and monolithic surface feature. The surface of MDPCT(W) (Fig. 6b) is also flat except for some cracks. The MDPCT(E) (Fig. 6c) exhibits a rough and flaky surface. For comparison, the bulk $CePO_4$:Tb (Fig. 6d) shows an obviously granular appearance. This suggests that water solvent can corroborate a combination of inorganic phosphinyl-cerium (terbium) and lead to a relatively integral and continuous organic–inorganic lamellar structure, while ethanol with weak polarity induces a loose structure and discontinuous surface. As far as we know, the formation of lamellar phases of MDPCT has hardly been reported, and this is a self-assembled, highly ordered layered structural and lamellar hybrid material.

The FT-IR spectra of MDP, MDPCT and bulk $CePO_4$:Tb are shown in Fig. 7. Alkyl chain vibrations υ_{CH} at 2960 cm^{-1}, 2920 cm^{-1}, 2852 cm^{-1} and δ_{CH} at 1470 cm^{-1} can be observed in the FT-IR spectra of surfactant containing materials, MDPCT(W,E) and MDP. The bands at 1625 cm^{-1} and 3500 cm^{-1} are assigned to bending and stretching vibrations of –OH. The $\upsilon_{(P–O)}$ band at 940–1200 cm^{-1} is visible for four samples, and this band of MDP

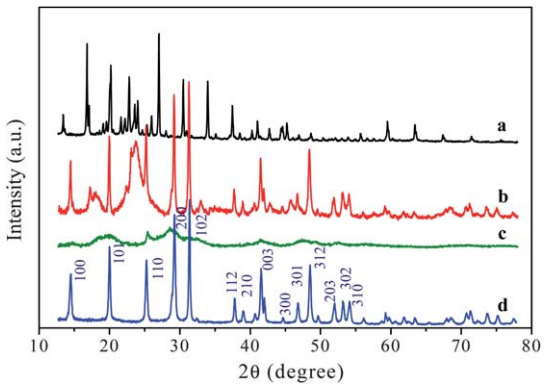

Fig. 4 Wide-angle XRD patterns of (a) MDP, (b) MDPCT(W), (c) MDPCT(E) and (d) bulk $CePO_4$:Tb.

and MDPCT(W,E) was affected by the alkyl chain, splitting into multiple peaks. The $\upsilon_{(P–O–C)}$ band at 728 cm^{-1} can observed in the MDP and MDPCT samples, but it cannot be found in the bulk $CePO_4$, which means that the inorganic phosphinyl-cerium (terbium) and dodecyl chain are linked by the P–O–C bond. It can also be proved by a quick delamination during the preparation process in polar solution (superstratum: MDPCT powder, and underlayer: clear solution). If the P–O–C bond was destroyed, the hydrolysate dodecanol would dissolve in polar solutions and the inorganic hydrolysate would be precipitated at the bottom. As the phenomenon above does not occur, it can validate that the P–O–C binding in MDPCT has formed. In the FT-IR spectrum of bulk $CePO_4$:Tb, the peaks at 612 cm^{-1} and 536 cm^{-1} can be attributed to the O–P–O bending vibrations (υ_2, υ_4) (Fig. 7d).[39,40] A couple of peaks at the same position can also be observed in the FT-IR spectra of MDPCT(W) and MDPCT (E) (Fig. 7b,c), but the intensities of peaks are weaker than that of bulk $CePO_4$:Tb. In Fig. 7b and 7c, there are several weak peaks at 420–630 cm^{-1}, and the peak at 536 cm^{-1} is a little stronger, which means that electric charge distribution in $C_{12}H_{25}$-OP(O)$O_2^{2-}\cdot Ce^{3+}$ is different from that in $P(O)O_3^{3-}\cdot Ce^{3+}$, and the former is influenced by alkyl and O–P–O bending vibrations.

Meanwhile, the O–P–O bending vibration of $C_{12}H_{25}$-OP(O)$O_2^{2-}\cdot Ce^{3+}$ in MPDCT(W,E) is different from that of $C_{12}H_{25}$-OP(O)$O_2^{2-}\cdot H^+$ in MPD (Fig. 7a), due to the presence of Ce^{3+} ions. For two MDPCT(W,E) samples, the O–P–O bending vibrations would be changed by an inductive effect from Ce^{3+}. Because of the different degrees of crystallinity in the two samples, the

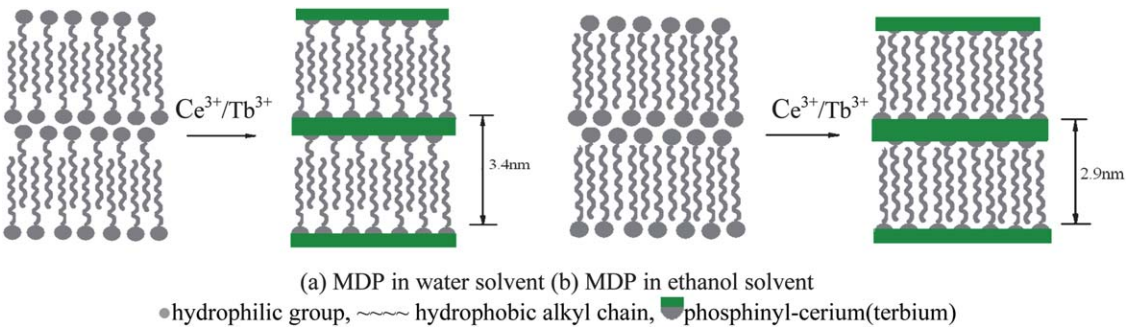

Fig. 3 Effect of solvent on the *d*-spacing in MDPCT during the preparation of MDPCT by MDP lamellar assembly.

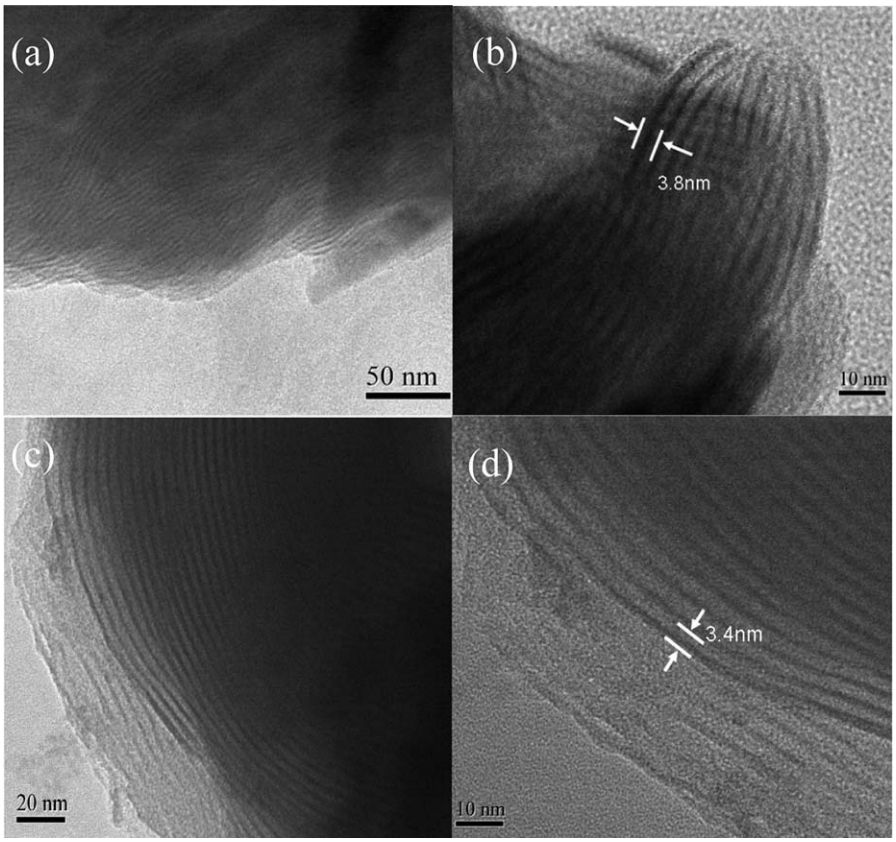

Fig. 5 TEM images of (a, b) MDPCT(W), and (c, d) MDPCT(E).

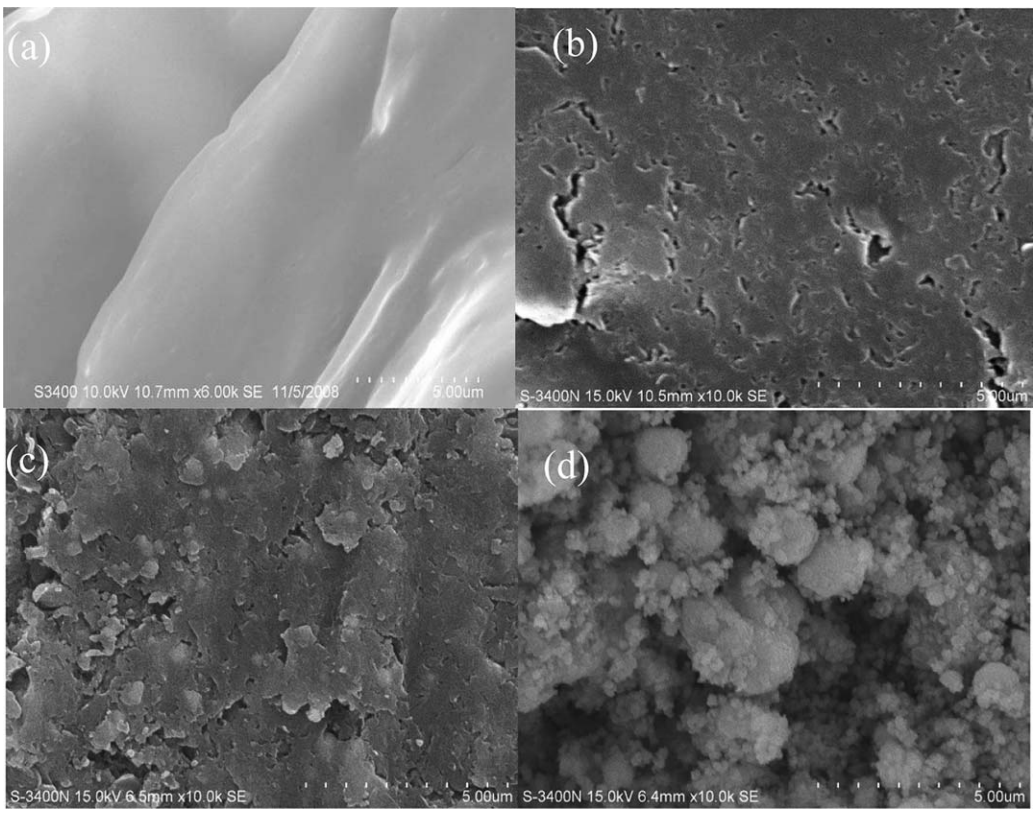

Fig. 6 SEM images of (a) MDP template, (b) MDPCT(W), (c) MDPCT(E), and (d) bulk $CePO_4$:Tb.

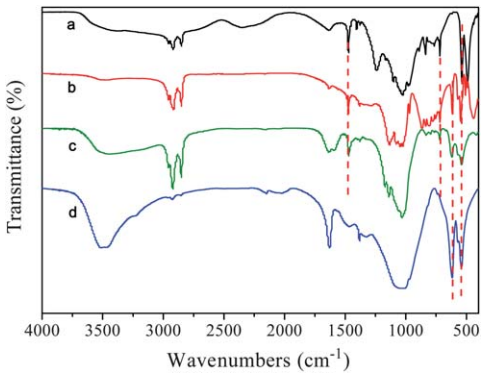

Fig. 7 FT-IR spectra of (a) MDP template, (b) MDPCT(W), (c) MDPCT(E), and (d) bulk $CePO_4$:Tb.

inductive effect of Ce^{3+} ions on $-OP(O)O_2^{2-}$ is different. Therefore, the intensity of the absorption band at 420–630 cm^{-1} is slightly different in MDPCT(W) and MDPCT(E). The peak at 440 cm^{-1} may be attributed to an effect of a $C_{12}H_{25}$-$OP(O)O_2^{2-}$ branching reaction, suggesting the existence of $C_{12}H_{25}$–$OP(O)$–$O_2 \cdot Ce \cdot O_2(O)PO$–$C_{12}H_{25}$. This peak is stronger in MDPCT(W) than in MDPCT(E), which supports the better crystallinity of inorganic phosphinyl-cerium in MDPCT(W) by the XRD results.

The above-mentioned results suggest that the cerium (terbium) ions affect the O–P–O bending vibrations in the hybrid materials, and their local environments are somewhat similar to that of bulk $CePO_4$:Tb, but not totally identical.

The photoluminescence (PL) spectra of MDPCT(W,E) and bulk $CePO_4$:Tb were measured at room temperature, and the results are presented in Figs. 8–10. In the MDPCT(W) excitation spectrum, the bands centred at 235, 254, and 295nm are due to the 4f–5d electronic transitions for Ce^{3+},[41,42] and the band positions in MDPCT(E) are little shifted. The excitation bands of bulk $CePO_4$:Tb are located at 235, 254, and 270 nm.[43] The excitation spectra of three samples under the emission of 345 nm (Fig. 9) show that the band positions are almost the same as in the excitation spectra under the emission of 545 nm in Fig. 8.

The emission spectra of the samples under the excitation of 254 nm are shown in Fig. 10, and the bands or peaks at 490, 545, 588, and 622 nm correspond to the transitions of $^5D_4$–$^7F_6$, $^5D_4$–$^7F_5$, $^5D_4$–$^7F_4$, and $^5D_4$–$^7F_3$, respectively. The green emission of the $^5D_4$–$^7F_5$ transition is stronger than the other transitions. The high intensity broad band at 300–400 nm results from the d–f transitions of Ce^{3+}. The cerium luminescence fails to be completely quenched by terbium, owing to the high concentration of Ce^{3+} in the MDPCT materials. These results indicate that an incomplete energy transfer from Ce^{3+} to Tb^{3+} occurs in MDPCT.[44] Thus, the MDPCT materials can emit blue and green light.

MDPCT(W) synthesized in water exhibits obviously higher emission intensity than MDPCT(E) synthesized in ethanol and bulk $CePO_4$:Tb. It suggests that water as a solvent is beneficial for the Ce^{3+} and Tb^{3+} ions bonding to $C_{12}H_{25}O$–$P(O)O_2^{2-}$. As shown in Fig. 11a, the polar water solvent exists in the space between the layers of hydrophilic group, the Ce^{3+} (Tb^{3+}) ions dissolved in water are between the adjacent two rows of hydrophilic groups, which is beneficial for the reaction of Ce^{3+}/Tb^{3+} and $-P(O)O_2^{2-}$, resulting in good crystallization of the inorganic part. In the ethanol solvent, partial solvent including $Ce^{3+}(Tb^{3+})$ ions can disperse in the alkyl chain, and C_2H_5O– would cause steric hindrance between $Ce^{3+}(Tb^{3+})$ and $-OP(O)O_2^{2-}$, weakening the effective reaction between the $Ce^{3+}(Tb^{3+})$ ions and hydrophilic groups as well as the crystallinity of phosphinyl-cerium (terbium) (Fig. 11b), which can be confirmed by the wide-angle XRD results.

MDPCT(W) and bulk $CePO_4$:Tb were synthesized in water, but bulk $CePO_4$:Tb displays a poor photoluminescence. According to the SEM, TEM and XRD results for the MDPCT and bulk $CePO_4$:Tb materials, we think that the high emission intensity of MDPCT(W) should be attributed to its particular and novel structure, ~3 nm crystallite wall in an ordered array, which is beneficial for the luminescence of rare earth ions due to a nano-effect, compared with the large particles (500 nm–5 μm) of bulk CePO4:Tb.[45–47] From the FT-IR results, it can be deduced that a stereo-effect of $C_{12}H_{25}$– in MDPCT(W) might affect the $-PO_4$ host, O–P–O vibration and the energy radiative transition, compared with bulk $CePO_4$:Tb.

To investigate the optimum Tb^{3+} dopant amount, the effect of Tb^{3+} concentration (mol %) on the photoluminescence properties of MDPCT(W) was studied and the results are shown in Fig. 12. When 5 mol% Tb^{3+} was added to MDPCT(W), the emission intensity reaches a maximum; when the Tb^{3+} amount is >5% or <5% in MDPCT(W), the emission intensity declines quickly

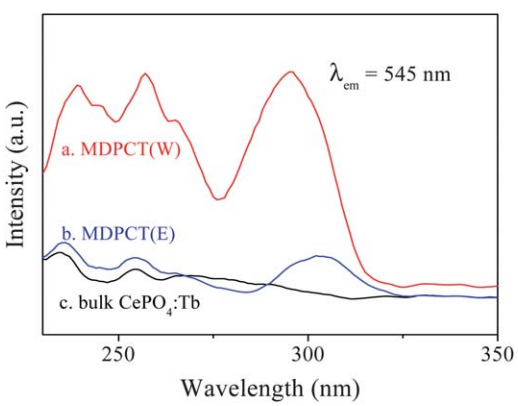

Fig. 8 Excitation spectra of (a) MDPCT(W), (b) MDPCT(E), and (c) bulk $CePO_4$:Tb.

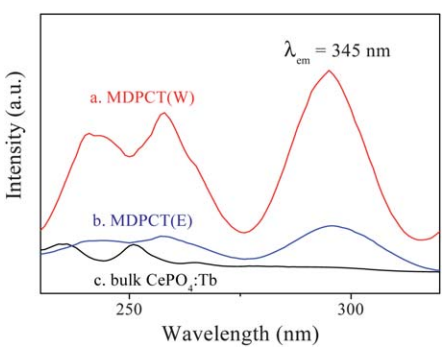

Fig. 9 Excitation spectra of (a) MDPCT(W), (b) MDPCT(E), and (c) bulk $CePO_4$:Tb, $\lambda_{em} = 345$ nm.

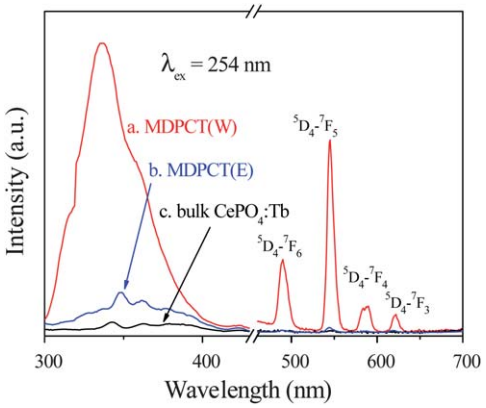

Fig. 10 Emission spectra of (a) MDPCT(W), (b)MDPCT(E), and (c) bulk $CePO_4$:Tb.

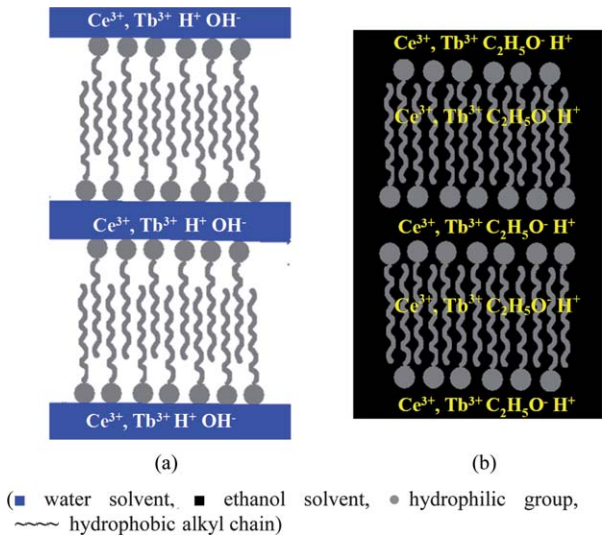

Fig. 11 Possible location of Ce^{3+}/Tb^{3+}ion in (a) water and (b) ethanol solvent, resulting in lamellar assembly with different degrees of crystallinity.

because of the concentration quenching effect. The effect of dopant Tb^{3+} concentration on the structure of MDPCT(W) was studied by small angle XRD, and the results (Fig. 13) show that the layered structure of the hybrid is hardly affected by the amount of Tb^{3+} dopant.

Fig. 14 shows the colour of MDPCT (W) dissolved in *n*-hexane under UV ($\lambda_{ex} = 250$nm) or natural daylight.

Conclusions

Photoluminescent lamellar organic–inorganic hybrid mono-n-dodecyloxy-phosphinyl-cerium (terbium) (MDPCT) materials have been successfully prepared by reacting mono-n-dodecyl phosphate with cerium (terbium) nitrate in water or ethanol solvent. The MDPCT materials are of an ordered layered structure with an ordered inter-lamellar spacing. The results show that the solvent obviously affects the structure and crystallization of synthesized MDPCT materials. MDPCT(W) prepared in water exhibits a more ordered layered structure and

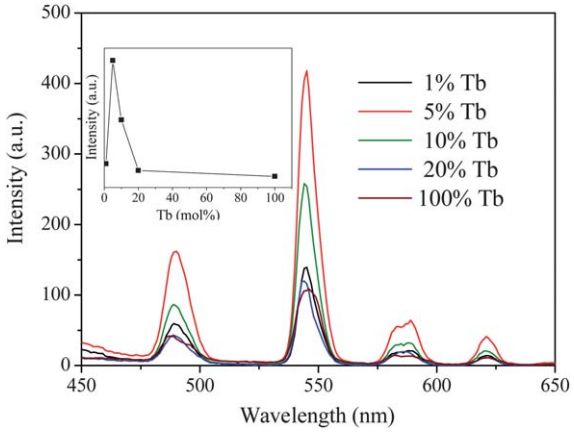

Fig. 12 Effect of Tb^{3+} concentration on photoluminescence properties of MDPCT(W).

a higher degree of crystallinity than MDPCT(E) prepared in ethanol. The inter-lamellar spacing of the former is 3.8 nm and the spacing of the latter is 3.4 nm. The MDPCT(W) sample exhibits stronger luminescent intensity than MDPCT(E). When the concentration of Tb^{3+} in MDPCT(W) is 5 mol%, its emission intensity of green light reaches a maximum.

In the preparation of MDPCT, MDP was used as both a phosphorus source and structural template, and the prepared MDPCT hybrid luminescent materials display many advanced characteristics: an ordered layered structure like that of cell membrane phospholipids, low toxicity compared with organic dyes and convenient preparation. This MDPCT hybrid luminescent material will be promising for potential biomedical applications in fluorescent imaging and analysis.

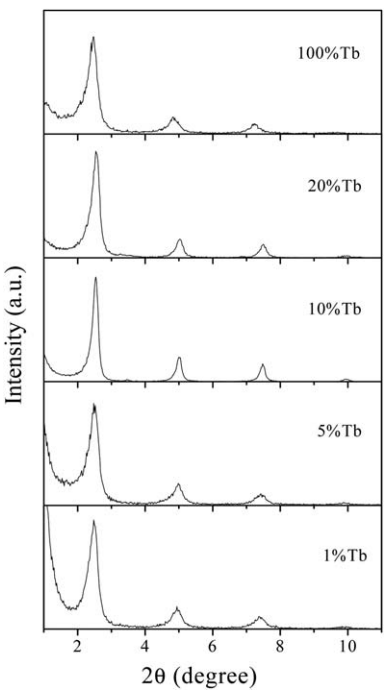

Fig. 13 Small-angle XRD patterns of different Tb^{3+} concentration of MDPCT(W).

Fig. 14 Color of MDPCT (W) dissolved in *n*-hexane (a) under UV (λ_{ex} = 250 nm), and (b) natural daylight.

Acknowledgements

This project was supported financially by the National Basic Research Program of China (2010CB732300), the "ShuGuang" Project (10GG23) and the Leading Academic Discipline Project (J51503) of Shanghai Municipal Education Commission and Shanghai Education Development Foundation.

Notes and references

1 M. Grätzel, *Nature*, 2001, **414**, 338.
2 M. A. Hickner, H. Ghassemi, Y. S. Kim, B. R. Einsla and J. E. McGrath, *Chem. Rev.*, 2004, **104**, 4587.
3 K. Adil, M. Leblanc, V. Maisonneuve and P. Lightfoot, *Dalton Trans.*, 2010, **39**, 5983.
4 P. Gomez-Romero, *Adv. Mater.*, 2001, **13**, 163.
5 K. N. Rao, L. D. Dingwall, P. L. Gai, A. F. Lee, S. J. Tavener, N. A. Young and K. Wilson, *J. Mater. Chem.*, 2008, **18**, 868.
6 P. M. Forster and A. K. Cheetham, *Top. Catal.*, 2003, **24**, 79.
7 S. Natarajan and S. Mandal, *Angew. Chem., Int. Ed.*, 2008, **47**, 4798.
8 Y. W. Tan, E. M. P. Steinmiller and K. S. Choi, *Langmuir*, 2005, **21**, 9618.
9 M. I. Khan, R. C. Nome, S. Deb, J. H. McNeely, B. Cage and R. J. Doedens, *Cryst. Growth Des.*, 2009, **9**, 2848.
10 A. K. Cheetham, C. N. R. Rao and R. K. Feller, *Chem. Commun.*, 2006, 4780.
11 A. C. Franville, D. Zambon, R. Mahiou and Y. Troin, *Chem. Mater.*, 2000, **12**, 428.
12 D. W. Dong, S. C. Jiang, Y. F. Men, X. L. Ji and B. Z. Jiang, *Adv. Mater.*, 2000, **12**, 646.
13 K. Binnemans, P. Lenaerts, K. Driesen and C. Gorller-Walrand, *J. Mater. Chem.*, 2004, **14**, 191.
14 P. N. Minoofar, B. S. Dunn and J. I. Zink, *J. Am. Chem. Soc.*, 2005, **127**, 2656.
15 L. N. Sun, H. J. Zhang, L. S. Fu, F. Y. Liu, Q. G. Meng, C. Y. Peng and J. B. Yu, *Adv. Funct. Mater.*, 2005, **15**, 1041.
16 Y. Wang, Y. Wang, P. P. Cao, Y. N. Li and H. R. Li, *CrystEngComm*, 2011, **13**, 177.
17 Y. Feng, H. R. Li, Q. Y. Gan, Y. G. Wang, B. Y. Liu and H. J. Zhang, *J. Mater. Chem.*, 2010, **20**, 972.
18 Y. J. Li, L. Wang and B. Yan, *J. Mater. Chem.*, 2011, **21**, 1130.
19 Y. J. Li and B. Yan, *J. Mater. Chem.*, 2011, **21**, 8129.
20 Q. M. Wang and B. Yan, *J. Mater. Chem.*, 2004, **14**, 2450.
21 M. A. Martin, A. I. Olives, B. del Castillo and J. C. Menendez, *Curr. Pharm. Anal.*, 2008, **4**, 106.
22 P. Escribano, B. Julian-Lopez, J. Planelles-Arago, E. Cordoncillo, B. Viana and C. Sanchez, *J. Mater. Chem.*, 2008, **18**, 23.
23 L. D. Carlos, R. A. S. Ferreira, V. D. Bermudez and S. J. L. Ribeiro, *Adv. Mater.*, 2009, **21**, 509.
24 K. Binnemans, *Chem. Rev.*, 2009, **109**, 4283.
25 N. Weibel, L. J. Charbonniere, M. Guardigli, A. Roda and R. Ziessel, *J. Am. Chem. Soc.*, 2004, **126**, 4888.
26 J. C. G. Bunzli, *Chem. Rev.*, 2010, **110**, 2729.
27 G. Z. Liu, C. E. Conn and C. J. Drummond, *J. Phys. Chem. B*, 2009, **113**, 15949.
28 W. S. Song, H. N. Choi, Y. S. Kim and H. Yang, *J. Mater. Chem.*, 20, p. 6929.
29 F. Duault, M. Junker, P. Grosseau, B. Guilhot, P. Iacconi and B. Moine, *Powder Technol.*, 2005, **154**, 132.
30 H. Lai, A. Bao, Y. M. Yang, Y. C. Tao, H. Yang, Y. Zhang and L. L. Han, *J. Phys. Chem. C*, 2008, **112**, 282.
31 P. Ghosh, A. Kar and A. Patra, *Nanoscale*, 2010, **2**, 1196.
32 O. M. Ntwaeaborwa, H. C. Swart, R. E. Kroon, P. H. Holloway and J. R. Botha, *J. Phys. Chem. Solids*, 2006, **67**, 1749.
33 Z. Y. Hou, L. L. Wang, H. Z. Lian, R. T. Chai, C. M. Zhang, Z. Y. Cheng and J. Lin, *J. Solid State Chem.*, 2009, **182**, 698.
34 A. K. Gulnar, V. Sudarsan, R. K. Vatsa, R. C. Hubli, U. K. Gautam, A. Vinu and A. K. Tyagi, *Cryst. Growth Des.*, 2009, **9**, 2451.
35 M. Fröba and M. Tiemann, *Chem. Mater.*, 1988, **10**, 3475.
36 S. M. Schmidt, J. McDonald, E. T. Pineda, A. M. Verwilst, Y. M. Chen, R. Josephs and A. E. Ostafin, *Microporous Mesoporous Mater.*, 2006, **94**, 330.
37 Y. J. Wu and S. Bose, *Langmuir*, 2005, **21**, 3232.
38 S. Z. Lin, Y. L. Yuan, H. T. Wang, R. K. Jia, X. F. Yang and S. J. Liu, *J. Mater. Sci.: Mater. Electron.*, 2009, **20**, 899.
39 M. Yang, H. P. You, Y. H. Zheng, K. Liu, G. Jia, Y. H. Song, Y. J. Huang, L. H. Zhang and H. J. Zhang, *Inorg. Chem.*, 2009, **48**, 11559.
40 L. Li, W. G. Jiang, H. H. Pan, X. R. Xu, Y. X. Tang, J. Z. Ming, Z. D. Xu and R. K. Tang, *J. Phys. Chem. C*, 2007, **111**, 4111.
41 J. R. Bao, R. B. Yu, J. Y. Zhang, X. D. Yang, D. Wang, J. X. Deng, J. Chen and X. R. Xing, *CrystEngComm*, 2009, **11**, 1630.
42 Y. P. Fang, A. W. Xu, R. Q. Song, H. X. Zhang, L. P. You, J. C. Yu and H. Q. Liu, *J. Am. Chem. Soc.*, 2003, **125**, 16025.
43 K. Riwotzki, H. Meyssamy, A. Kornowski and M. Haase, *J. Phys. Chem. B*, 2000, **104**, 2824.
44 G. Z. Chen, S. X. Sun, W. Zhao, S. L. Xu and T. You, *J. Phys. Chem. C*, 2008, **112**, 20217.
45 W. U. Huynh, J. J. Dittmer and A. P. Alivisatos, *Science*, 2002, **295**, 2425.
46 J. Wang, M. S. Gudiksen, X. Duan, Y. Cui and C. M. Lieber, *Science*, 2001, **293**, 1455.
47 H. Choi, J. H. Kim, S. S. Yi, B. K. Moon and J. H. Jeong, *J. Alloys Compd.*, 2006, **408**, 816.

